Photofragment spectroscopy of shape resonances in OH^+

H. Helm, P. C. Cosby, and D. L. Huestis
Molecular Physics Department, SRI International, Menlo Park, California 94025
(Received 21 February 1984)

Discrete transitions are observed in an OH^+-ion beam which lead to predissociation into $O^+ + H$. The transitions are assigned to the $A\,^3\Pi \leftarrow X\,^3\Sigma^-$ system leading to quasibound levels supported by the $\Omega=2$ and $\Omega=1$ substates of $A\,^3\Pi$. The observed predissociation manifests the action of long-range dynamic coupling in the $O^+ + H$, $O + H^+$ charge-transfer channels. Improved values for the bond energy of OH^+ and the ionization potential of OH are obtained.

I. INTRODUCTION

The charge-transfer reaction $O + H^+ \rightarrow O^+ + H$ is the first step in the interstellar chemical cycle leading to the formation of OH.[1] The reverse reaction represents the major ionization source for atomic hydrogen in the earth's ionosphere.[2] The high rate at which this reaction proceeds in either direction derives in part from the accidental coincidence between the dissociation limits $O(^3P_1)+H^+$ and $O^+(^4S^o)+H(^2S)$, which are degenerate within the current knowledge of the ionization potentials of atomic oxygen and hydrogen[3] (see Fig. 1). The importance of the charge-exchange reaction has triggered a number of theoretical investigations, the most fundamental being the close-coupling calculations by Chambaud *et al.*[4] who explicitly included the fine-structure excitation in the charge-exchange channel. These authors showed that the charge-transfer event arises from dynamical coupling among the OH^+ molecular states at large internuclear separations (4–6 Å), with enhancement in the cross section at specific energies corresponding to shape resonances in the $A\,^3\Pi$ state. Here we report a first experimental study of two such resonances, which in a molecular picture may be viewed as quasibound levels of the adiabatic fine-structure states of $A\,^3\Pi$ shown in Fig. 1. The levels are excited from the $X\,^3\Sigma^-$ ground state in a mass-selected OH^+-ion beam with a cw uv laser. The dissociative decay of these resonances into $O^+ + H$ is monitored by observation of the charged photofragments and measurement of their kinetic energy distribution. Analysis of the excitation spectrum, the photofragment separation energies, and the excitation linewidths of the resonances allows the assignment of quantum numbers to the resonances and a first direct measurement of the dissociation energy of OH^+.

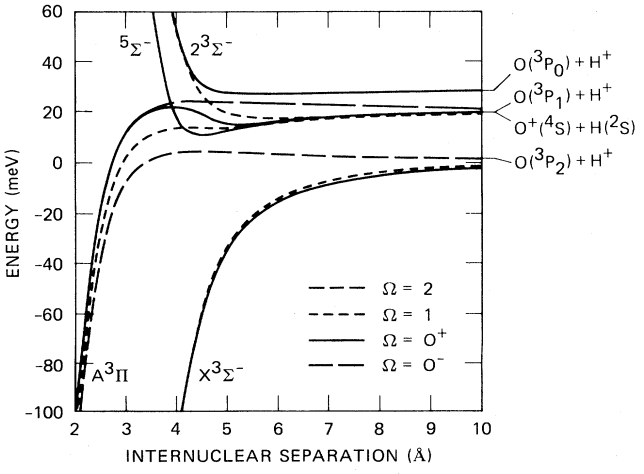

FIG. 1. Asymptotic rotationless potential curves for OH^+, with energies expressed relative to $O(^3P_2)+H^+$.

II. EXPERIMENTAL

The apparatus, a laser-ion coaxial beams–photofragment spectrometer, has been described in detail previously,[5] as has its application to spectroscopic studies.[6] The OH^+ was produced by dissociative electron-impact ionization of water vapor and accelerated to a specified energy between 2 and 4 keV. The mass-selected and collimated ion beam was merged with the laser beam over a distance of 50 cm. The argon-ion laser used in this work provided six discrete wavelengths in the uv: 3638, 3511, 3514, 3358, 3345, and 3336 Å. External prisms were used to select the wavelength, which was then calibrated against a stabilized HeNe laser. Transitions in OH^+ were velocity-tuned into resonance with the fixed laser frequency by varying the velocity of the OH^+ beam in the laser interaction region. By directing the laser both parallel and antiparallel to the ion beam, ten spectral regions were investigated, each covering approximately 7–10 cm^{-1} in width. The O^+ photofragments produced in photodissociation of OH^+ were deflected into an energy analyzer and detected by a channeltron. Energy analysis of the photofragments allowed determination of the energy of the dissociated levels above the dissociation limit, called the separation energy W.

Seven discrete transitions and a weak continuous background were observed to lead a photodissociation into $O^+ + H$. Figure 2 shows a typical wavelength scan for $W=0$ obtained using the single-frequency output of the Ar-ion laser at 3514 Å and tuning the OH^+ beam energy from 2000 to 2500 eV. The insets give the kinetic energy spectra of the O^+ photofragments obtained from the two transitions. The discrete separation energy of the pho-

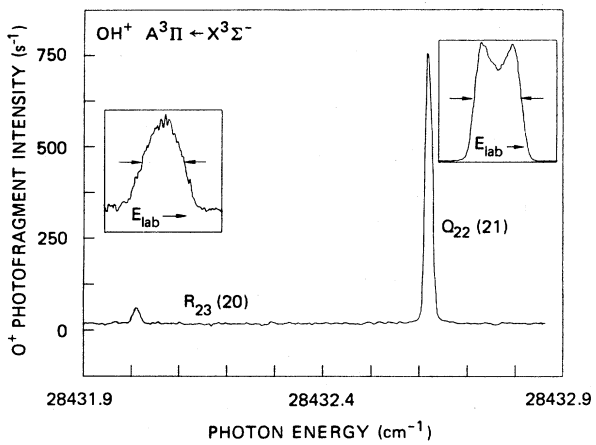

FIG. 2. Variation in O^+ photofragment intensity from the photodissociation of OH^+ as a function of photon energy. Two transitions in the $A\,^3\Pi\ (v=5) \leftarrow X\,^3\Sigma^-\ (v=2)$ band appear in this portion of the spectrum. The laboratory kinetic energy spectra of the O^+ photofragments arising from each transition are shown as insets. The underlying background in the kinetic energy spectrum of the $R_{23}(20)$ transition is due to the near coincidence at this photon energy of a $c\,^1\Pi \leftarrow a\,^1\Delta$ transition labeled *h* in Table I.

tofragments in the center-of-mass frame is determined from the width of the kinetic energy distributions measured at half height. The experimental parameters determined for the observed transitions are compiled in Table I.

The transition linewidths (Γ) are determined from the breadth of the absorption peaks at half maximum. They are wider than the apparatus limited width ($\sim$100 MHz) and hence reflect the predissociation lifetimes of the excited levels involved.

An attempt was made to observe H^+ photofragments. To our surprise none were found. We now understand that the failure to observe H^+ is due to the greatly differing sensitivities of the photofragment spectrometer in detecting O^+ and H^+ fragments. To discuss the detection sensitivity we must examine the spatial distribution of photofragments, which is illustrated in Fig. 3. The primary ion beam is merged with the laser beam in the first electrostatic quadrupole element Q_1. In the region between the two quadrupoles, the laser with its polarization perpendicular to the parent beam velocity excites primary beam molecules to predissociated levels. Emerging from this event, the fragment velocity is a sum of the original beam velocity and a component from the separation energy. This latter component causes a shift in the laboratory energy and angle of each fragment, the laboratory distributions depending on the center-of-mass angular distribution of the photofragments. Shown in Fig. 3 are two extremes of such distributions, $\sin^2\theta$ and $\cos^2\theta$, labeled parallel and perpendicular, respectively. The true distributions produced depend upon the various angular momentum quantum numbers of the states involved and their lifetimes and lie somewhere between these two extreme values. In the second quadrupole one of the photofragments (H^+ or O^+) is energy selected and thus separated from the remainder of the beam. The proton fragments are centered around $\frac{1}{17}$th of the primary beam energy, the oxygen fragments around $\frac{16}{17}$th of the primary beam energy. Owing to the imparted separation energy most of the fragments will spread around the original beam direction, preferentially collecting within a circle with a radius determined by the ratio of center-of-mass speed of the separating fragments to the primary beam speed and the distance from the dissociation region. The two spatial distributions shown in Fig. 3 were obtained by a Monte Carlo calculation of actual apparatus trajectories accounting for realistic operating conditions such as a finite beam size, and interaction length, as well as dispersion effects in Q_2. To understand the greatly different sensitivity for proton and oxygen fragments we have to recall that only a small fraction of the spatial distribution of photofragments is accepted into the electrostatic energy analyzer which is situated about 170-cm downstream from the second quadrupole and has an acceptance aperture of 1-mm diameter. For an example we assume a pri-

TABLE I. Transitions to discrete, predissociated levels observed in OH^+.

Label	$h\nu$ (cm^{-1})	W (meV)	Γ (MHz)	Observed intensity	Calculated intensity	Assignment	(v',v'')
group I						$A \leftarrow X$	
a	28432.01	40	550	1	1	$R_{23}(20)$	(5,2)
b	28432.62	40	550	15	41	$Q_{22}(21)$	(5,2)
c	28437.40	~40	~550	1	1.1	$P_{21}(22)$	(5,2)
group II						$A \leftarrow X$	
d	29948.16	34	4500	1	1	$Q_{12}(18)$	(6,2)
e	29952.76	34	4500	5	9.9	$P_{11}(19)$	(6,2)
f				not observed	0.01	$R_{13}(17)$	(6,2)
group III						$c \leftarrow a$	
g	28454.39	800	225				(0,0)[a]
h	28432.01	750	<550				(0,0)[a]

[a]Tentative assignment.

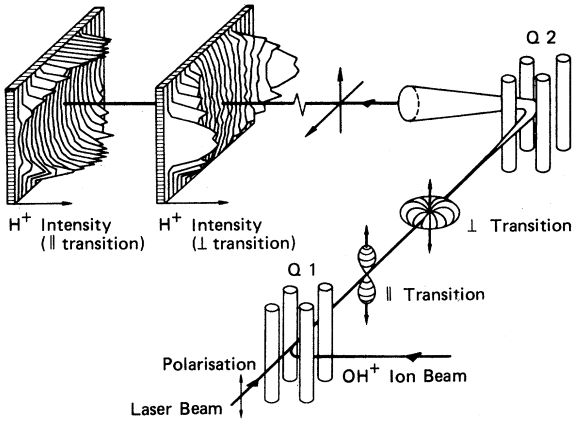

FIG. 3. Schematic of spatial distribution of H^+ photofragments produced from parallel and perpendicular transitions in OH^+.

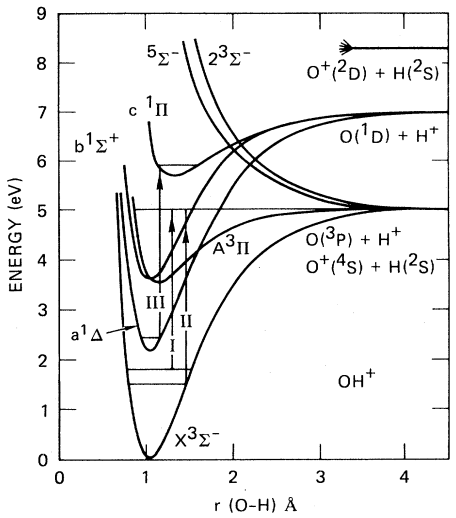

FIG. 4. Low-lying electronic states of OH^+ from Ref. 3 and 7. The three groups of observed transitions listed in Table I are indicated by I, II, and III in this figure.

mary beam energy of 3000 eV and a separation energy of $W=40$ meV. A simple calculation for the spatial distribution of fragments after 200 cm of flight path shows that oxygen fragments will fall into a ring of ~2-mm diameter. By contrast proton fragments, which due to their lower mass carry most of the separation energy, will spread much farther around the beam, into a ring of ~30 mm. As a result the number of proton fragments falling into the aperture of the energy analyzer is an order of magnitude below that of the oxygen fragments. We believe that this discrimination is the origin for our inability to date to detect proton fragments from the predissociating transitions given in Table I.

A more sensitive scheme for detecting the proton fragments is being developed. The current paper describes results and interpretations derived from the detection of the oxygen-ion fragment alone.

III. IDENTIFICATION OF TRANSITIONS

A. $A\,^3\Pi \leftarrow X\,^3\Sigma^-$ transitions

As can be seen in Table I the measured linewidths and separation energies are, within their experimental uncertainties, identical among the three transitions *a*, *b*, and *c* (group I), and the two transitions labeled *d* and *e* (group II), respectively. Both linewidth and separation energy are attributes of the upper electronic state involved and hence these results suggest that all transitions within each group access a similar (or the same) predissociated level in the upper state. If we assume that the dissociation occurs to the lowest dissociation limit, $O^+(^4S^0_{3/2})+H(^2S)$, the lower electronic state involved in transitions observed in both groups I and II has, for energetic reasons, to be $X\,^3\Sigma^-$ (see Fig. 4). The observed spacings of the transitions in both groups (0.61 and 4.80 cm^{-1} in group I and 4.60 cm^{-1} in group II) are consistent with the expected spin splitting of levels in the $X\,^3\Sigma^-$ ground state of OH^+, but are much smaller than the rotational spacing in the ground state. This further suggests that within each group the transitions access a single quasibound level from the spin-split components of a single rotational level of the ground state $X\,^3\Sigma^-$. The energetic location of these rotational levels relative to the dissociation limit $O^+ + H$ may be obtained by subtracting the measured separation energies from the transition energies. The lower-state levels involved in the group-I transitions lie $28\,080\pm30$ cm^{-1} below the dissociation limit, whereas those of group II lie $29\,678\pm30$ cm^{-1} below this limit. The stated uncertainties arise from the uncertainty in the experimental measurement of *W*. Using the bond energy[8–10] of the OH^+ ground state, $40\,446\pm90$ cm^{-1}, the rovibrational energy of the rotational levels (relative to the lowest existing level in the ground state) are $12\,366\pm120$ (group I) and $10\,768\pm120$ cm^{-1} (group II). The relative location of the lower-state levels is shown in Fig. 4.

Merer *et al.*[11] have studied the *A*-*X* system of OH^+ in emission, and have analyzed rovibrational levels of the ground state up to 9700-cm^{-1} excitation energy, covering the ground-state vibrational levels $v''=0$, 1, and 2. Extrapolation of their levels using their molecular constants into the energy range observed here shows that two rovibrational levels with the required lower-state spacing fall into the range of dissociation energies for groups I and II. These levels are $v''=2$, $N''=21$ (12 304 cm^{-1}), and $v''=2$, $N''=18$ (10 677 cm^{-1}). Since it is unlikely that the extrapolated rotational spacing is in error by as much as 100 cm^{-1} the assignment of lower-state levels to $v''=2$, $N''=18$ and 21 is firm, provided the bond energy of OH^+ is correct within the uncertainties stated in previous work.[9,10]

Assuming that an allowed electronic transition is observed, the upper electronic state accessed by the transitions in groups I and II has to be the $A\,^3\Pi$ state which correlates adiabatically to the $O(^3P)+H^+$ limit. Three pieces of experimental information are available which facilitate the assignment of quantum numbers to the predissociated levels. First, the kinetic energy distributions (see as example Fig. 2) identify[12] the transitions labeled *b* and *d* in Table I as *Q*-type transitions ($J'-J''=0$), the

remainder being of type R or P ($J'-J''=\pm 1$). Second, the observed relative intensities show that in group I the Q transition is strong while in group II the strong transition is either type P or R (see Table I). A third source of information comes from the spin splitting of the lower-state levels involved. In Fig. 5 we show the transitions of group I and group II on a molecular energy scale. Since the ordering of fine-structure levels in the $^3\Sigma^-$ ground state has been established by the work of Merer *et al.*,[11] we can identify the lower fine-structure levels involved in the Q-type transitions of groups I and II as F_2'' ($N''=J''$). The similarities among the transition linewidths and among the separation energies observed for transitions in each group suggest that each group accesses a single predissociated level, thus requiring the assignment of the remaining transitions as P type (for transitions d and e) and R type (transition b), with the R-branch transition of group II being conspicuously absent in the experiment.

We have calculated the intensity distribution of the 27 possible branches in the OH^+ $A\,^3\Pi$-$X\,^3\Sigma^-$ transition using Merer's molecular constants and the computer program RLS kindly provided by Albritton.[13] We find that, in order to reproduce the observed intensity distribution, the upper-state fine-structure level for group I has to be assigned to F_1' [corresponding to $^3\Pi_2$ in Hund's case (a)] while it has to be $F_2'(^3\Pi_1)$ for the transitions in group II. The calculated intensities and observed, normalized intensities for the assigned transitions are given in Table I. It may be seen that the third transition expected for group II, $R_{13}(17)$, has a predicted intensity 100 times smaller than that of transition $Q_{12}(18)$. Since the count rate for the latter transition amounted to as little as 30 counts/s, the $R_{13}(17)$ transition expected for group II remained undetected. We note from Table I that the predicted intensities for the strong transitions are higher than those observed by factors of 2 and 3. One possible explanation for this disagreement is saturation of the transitions (the ions are illuminated with single-frequency radiation at power levels of typically 50 W/cm^2 for several μs).

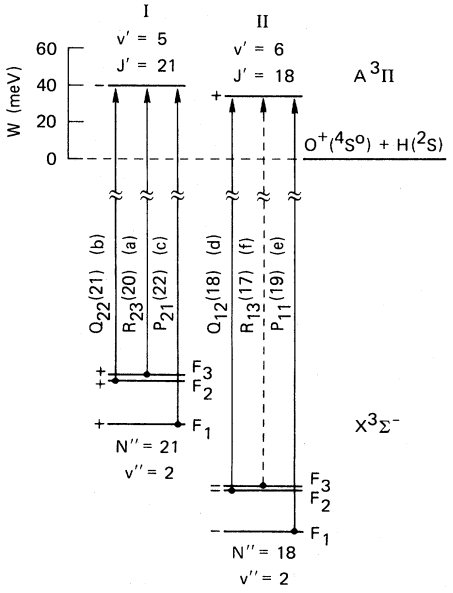

FIG. 5. Energy-level diagram of rotational transitions observed in groups I and II.

The vibrational assignments in the upper state can be made by extrapolating the known high-J' energy levels for the $A\,^3\Pi$ state ($v'=0-2$ for OH^+ and $v'=0-3$ for OD^+, from Ref. 12) to the energetic dissociation limit. This led to assignment of $v'=6$ and 5 for groups I and II, respectively.

B. Remaining transitions

The two transitions observed in group III appear with separation energies too high to be supported by the $A\,^3\Pi$ state. A tentative assignment of these transitions to the $c\,^1\Pi$-$a\,^1\Delta$ system can be made on the basis of the following argument: Subtracting the separation energy from the transition energy we find the lower-state levels involved in transitions g and h to lie 22100 ± 600 cm^{-1} below the dissociation limit. If this limit is assumed to be $O^+(^4S^o)+H(^2S)$ the lower-state levels involved are calculated to lie 2.46 ± 0.07 eV above the bottom of the well of the OH^+ ground state (see Fig. 4). The OH photoelectron spectrum obtained by Katsumata and Lloyd[10] places the lowest vibrational level in the $a\,^1\Delta$ state at 2.19 eV. The deperturbation study in the A-X system of OD^+ by Merer *et al.*,[11] when combined with the photoelectron results, places this level in OH^+ at 2.175 eV. Thus rotational levels of $a\,^1\Delta(v=0)$ with $J\approx 11$ are expected to lie in the energy range required for the transitions g and h. The $c\,^1\Pi$ state in OH^+ has never been observed experimentally; however, the calculations of Liu and Verhaegen[7] place the lowest vibrational level in this state $\sim$800 meV above the lowest dissociation limit. The group-III transitions are thus consistent with the expected energies for transitions in the $c\,^1\Pi \leftarrow a\,^1\Delta$ system of OH^+. However, the two transitions g and h do not provide sufficient information to uniquely assign the vibrational and rotational quantum numbers involved.

IV. DISCUSSION

The assignment of the transitions in groups I and II warrants a further analysis of the bond energy of OH^+ and a discussion of the dissociation mechanism involved in the observed fragmentation into $O^+ + H$. Based on our lower-state assignment, an independent value of the bond energy of OH^+ can be derived from the current observations using the measured separation energies. In order to do so, the rotational constants for the ground state as obtained by Merer *et al.*[11] have to be used to extrapolate from the highest previously observed rotational levels (at 9700 cm^{-1}) to the levels involved here (at 10 700 and 12 300 cm^{-1}, respectively). A value of $40\,384\pm45$ cm^{-1} is obtained, where the stated error limits do not include a small, but unknown uncertainty arising from the extrapolation. Using this value for the bond energy in a thermodynamic cycle, an adiabatic ionization potential of OH of $104\,873\pm60$ cm^{-1} is obtained, the additional 15 cm^{-1} uncertainty arising from the uncertainty in the bond energy[9] of neutral OH. The direct measurement of the vertical ionization potential by Katsumata and Lloyd[10] gave a value of 104 931 cm^{-1}; the appearance potential measure-

TABLE II. Model spin-rotation Hamiltonian for OH^+.

		$\Omega=2^a$		$\Omega=1$			$\Omega=0^+$			$\Omega=0^-$	
		$^3P_2^2$	$^5\Sigma_2^-$	$^3P_2^1$	$^3P_1^1$	$^5\Sigma_1^-$	$^3\Sigma_1^-$	$^3P_2^0$	$^3P_0^0$	$^3\Sigma_0^-$	$^3P_1^0$	$^5\Sigma_0^-$
$\Omega=2$	$^3P_2^2$	$a+b+P_2-2B$	0	f	0	0	0	0	0	0	0	0
	$^5\Sigma_2^-$	0	$c+e+S-2B$	0	0	f	0	0	0	0	0	0
$\Omega=1$	$^3P_2^1$	f	0	$a-\frac{b}{2}+P_2+4B$	$-\frac{3}{2}b$	0	$d/\sqrt{2}$	$\sqrt{3}g$	0	0	0	0
	$^3P_1^1$	0	0	$-\frac{3}{2}b$	$a-\frac{b}{2}+P_1$	0	$d/\sqrt{2}$	0	0	0	g	0
	$^5\Sigma_1^-$	0	f	0	0	$c+e+S+4B$	0	0	0	0	0	$\sqrt{3}g$
	$^3\Sigma_1^-$	0	0	$d/\sqrt{2}$	$d/\sqrt{2}$	0	$c+S$	0	0	g	0	0
$\Omega=0^+$	$^3P_2^0$	0	0	$\sqrt{3}g$	0	0	0	$a-b+P_2+6B$	$\sqrt{2}b$	$2d/\sqrt{6}$		
	$^3P_0^0$	0	0	0	0	0	0	$\sqrt{2}b$	$a+P_0$	$-d/\sqrt{3}$		
	$^3\Sigma_0^-$	0	0	0	0	0	g	$2d/\sqrt{6}$	$-d/\sqrt{3}$	$c+S+2B$		
$\Omega=0^-$	$^3P_1^0$	0	0	0	g	0	0				$a+b+P_1+2B$	0
	$^5\Sigma_0^-$	0	0	0	0	$\sqrt{3}g$	0				0	$c+e+S+6B$

[a]For e levels include $\Omega=2,1,O^+$. For f levels include $\Omega=2,1,O^-$. Parameter values are given in Table III.

ment of OH^+ in the photoionization of H_2O provided an upper limit[14] for the ionization potential of $104\,811\pm75$ cm^{-1}. Our value is consistent with both of these previous values for the OH ionization potential and thus our bond-energy value represents an improvement over the previous, indirect values of the bond energy of OH^+. The combination of all of these values, assuming an uncertainty of ±80 cm^{-1} in the dissociation energy derived from the work of Katsumata and Lloyd, yields a "best" value for the ionization energy of OH of $104\,866\pm20$ cm^{-1}.

The potential energy curves shown in Figs. 1 and 4 suggest that the observed quasibound levels are trapped behind the rotational barrier in the $A\,^3\Pi$ state, and that tunneling through the barrier may be a plausible predissociation mechanism. The potential energy curves shown in Fig. 1 were constructed by diagonalizing the asymptotic rotationless model Hamiltonian for OH^+, following exactly the work of Gentry and Giese[15] and Chambaud *et al.*,[4] including the known polarizabilities of O and H, quadrupole moment of O, and spin-orbit coupling in O, and assumed[4] charge-exchange matrix elements between the $^3\Sigma^-$ states arising from $O+H^+$ and O^++H, and exponential repulsion in the $^5\Sigma^-$ state. Inclusion of off-diagonal coriolis couplings is straightforward in the atomic basis.[16] This allows us to set up the asymptotic spin-rotation Hamiltonian which we give in Tables II and III, and to calculate rotationally adiabatic potential-energy curves for both e- and f-parity levels.[17] Such calculations, which are illustrated in Fig. 6 for $J=18$ e-parity levels, show rotational barriers of 60 and 120 meV (above O^++H) for $^3\Pi_2$ ($J=18$) and $^3\Pi_1$ ($J=21$), respectively. These barriers are sufficiently high to support the levels

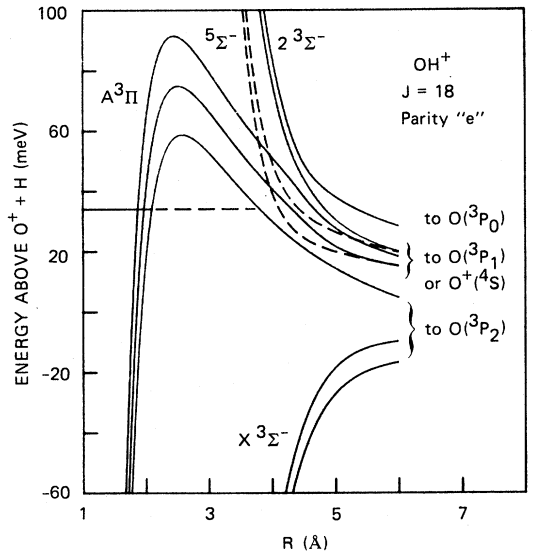

FIG. 6. Asymptotic rotationally adiabatic OH^+ potential-energy curves for parity e levels with $J=18$. The solid curves are eigenvalues of the spin-rotation Hamiltonian in Table II. The $^5\Sigma^-$ curves, given by the dashed lines, were calculated separately because they are not mixed with other levels by this Hamiltonian. The solid and dashed horizontal line segments give the energetic location of $v=6$ in the bound and barrier regions, respectively, of the $A\,^3\Pi_1$ substate. All energies are referenced to the $O^+(^4S)+H$ separated atom limit.

TABLE III. Hamiltonian parameters for OH^+.

Symbol	Expression[a]	Description
$a(R)$	$=-\frac{q^2}{6R^4}(2\alpha_\Pi^0+\alpha_\Sigma^0)=-\frac{5.770}{R^4}$	O-atom spherical charge-induced dipole[b]
$b(R)$	$=-\frac{qQ^0}{4R^3}-\frac{q^2}{6R^4}(\alpha_\Pi^0-\alpha_\Sigma^0)$	O-atom charge-quadrupole plus anisotropic charge-induced dipole[b]
	$=\frac{1.612}{R^3}-\frac{0.0336}{R^4}$	
$c(R)$	$=-\frac{q^2}{2R^4}\alpha^H=-\frac{4.799}{R^4}$	H-atom charge-induced dipole[c]
$d(R)$	$=69.3\exp(-1.70R)$	Charge exchange[c]
$e(R)$	$=16382\exp(-3.46R)$	Quintet repulsion[c]
$g(R)$	$=2B(R)\sqrt{J(J+1)}$	Off-diagonal rotational coupling
$f(R)$	$=2B(R)\sqrt{J(J+1)-2}$	
$B(R)$	$=\frac{\hbar^2}{2\mu R^2}=\frac{2.204\times10^{-3}}{R^2}$	Rotational constant
P_2	$=-19.62\times10^{-3}$	Asymptotic energies[d] for $O+H^+$
P_1	$=1.1\times10^{-6}$	
P_0	$=8.520\times10^{-3}$	
S	$=0$	Asymptotic energy[d] for O^++H

[a]Energies in eV, distances in Å.
[b]Reference 15.
[c]Reference 4.
[d]Reference 3.

observed here. By integrating $[V(R)-E]^{1/2}$ we calculated semiclassical lifetimes against barrier penetration[18] and found that in the former case the barrier height and width are consistent with the observed linewidths (group II of Table I). In group I, however, the barrier calculated for $^3\Pi_1$ is found to be too high for tunneling to be the only predissociation mechanism.

Having rationalized the existence of quasibound levels in the $A\,^3\Pi$ state of OH^+, we next seek to identify the mechanism by which these levels can dissociate to O^++H. Diabatically, all components of the $A\,^3\Pi$ state are derived from the neutral oxygen dissociation limit. The adiabatic correlations are more complicated. Given the assumed degeneracy of the $O(^3P_1)+H^+$ and $O^+(^4S)+H$ dissociation limits, and including all interactions, only two definite conclusions can be reached: the $\Omega=2$ component must correlate to $O(^3P_2)$, while all other components must lead to either $O(^3P_1)$ or $O^+(^4S)$. Our observation of O^+ fragments from excitation of both the $^3\Pi_2$ and $^3\Pi_1$ states confirms the importance of both spin-orbit and rotational coupling between the Π and Σ states. For example, the $^3\Pi_2$ could yield O^+ by two mechanisms: (1) weak spin-orbit interaction with $^5\Sigma^-$ near 4 Å (which we have not included in Table II because there is no first-order matrix element) or (2) it could mix with $^3\Pi_1$ by rotational coupling near 4 Å and mix a second time with $^3\Sigma^-$ by spin orbit and charge transfer. We note that the rotational-coupling matrix element between the two $^3\Pi$ states (labeled f in Table II) amounts to 40 cm^{-1} at 4 Å. With potential-energy curves that are only qualitatively reasonable, and with only the limited experimental data, we cannot make more quantitative statements at this time. By detecting both the O^+ and H^+ fragments we would be able to establish the branching between the four possible dissociation limits, which should reveal a more detailed view of the dynamics of predissociation, and of the reverse process, charge exchange.

V. CONCLUSION

The observation of predissociation of quasibound levels in the $A\,^3\Pi$ state now opens the possibility of an experimental study of the long-range interactions in OH^+, similar to our previous studies[19,20] in O_2^+ and N_2^+. Our observation of fragmentation into the O^+ channel is direct evidence for the action of nonadiabatic couplings between the $^3\Pi$ potential and the $^{3,5}\Sigma^-$ states which correlate to the $O^+(^4S^0)+H(^2S)$ limit. A first search for photofra-

ments reaching the $H^+ + O(^3P)$ channel has been unsuccessful, due to the low sensitivity of the present configuration to detect a light photofragment from a heavy diatomic. We are currently working on an improved detection scheme to study the branching among the four dissociation channels.

ACKNOWLEDGMENTS

This research was supported by the National Science Foundation under Grant No. PHY-81-12534 and by the U. S. Air Force Office for Scientific Research (AFOSR) under Contract No. F49620-81-K0006.

[1]J. H. Black and A. Dalgarno, Astrophys. J. Suppl. **34**, 405 (1977).

[2]R. F. Stebbings, A. C. H. Smith, and H. Erhardt, J. Geophys. Res. **68**, 2349 (1967).

[3]C. E. Moore, *Ionization Potentials and Ionization Limits Derived from the Analysis of Optical Spectra,* Natl. Stand. Ref. Data Ser., Natl. Bur. Stand. (U.S.), Circ. No. 34 (U.S. GPO, Washington, D.C., 1970).

[4]G. Chambaud, J. M. Launay, B. Levy, P. Millie, E. Roueff, and F. Tran Minh, J. Phys. B **13**, 4205 (1980).

[5]B. A. Huber, T. M. Miller, P. C. Cosby, H. D. Zeman, R. L. Leon, J. T. Moseley, and J. R. Peterson, Rev. Sci. Instrum. **48**, 1306 (1977).

[6]P. C. Cosby, J. B. Ozenne, J. T. Moseley, and D. L. Albritton, J. Mol. Spectrosc. **79**, 203 (1980).

[7]M. P. D. Liu and G. Verhaegen, Int. J. Quantum Chem. **5**, 103 (1971).

[8]The bond energy is obtained from the spectroscopic bond energy of the OH ground state (Ref. 9) and the spectroscopic measurement of the ionization potentials of OH (Ref. 10) and of atomic oxygen (Ref. 3).

[9]C. Carlone and F. W. Dalby, Can. J. Phys. **47**, 1945 (1969).

[10]S. Katsumata and D. R. Lloyd, Chem. Phys. Lett. **45**, 519 (1977).

[11]A. J. Merer, D. N. Malm, R. W. Martin, M. Horani, and J. Rostas, Can. J. Phys. **53**, 251 (1975).

[12]H. Helm, P. C. Cosby, M. M. Graff, and J. T. Moseley, Phys. Rev. A **25**, 304 (1982).

[13]D. L. Albritton (private communication).

[14]K. E. McCulloh, Int. J. Mass Spectrom. Ion Phys. **21**, 333 (1976).

[15]W. R. Gentry and C. F. Giese, J. Chem. Phys. **67**, 2355 (1977).

[16]V. Aquilanti and G. Grossi, J. Chem. Phys. **73**, 1165 (1980).

[17]H. Helm, P. C. Cosby, R. P. Saxon, and D. L. Huestis, J. Chem. Phys. **76**, 2516 (1982).

[18]R. J. LeRoy and W.-K. Liu, J. Chem. Phys. **69**, 3622 (1978).

[19]H. Helm, P. C. Cosby, and D. L. Huestis, J. Chem. Phys. **73**, 2629 (1980).

[20]H. Helm and P. C. Cosby, J. Chem. Phys. **76**, 4720 (1982).